Journal of the American College of Cardiology Vol. 52, No. 24, 2008

Published by Elsevier Inc.
ISSN 0735-1097/08/$34.00
doi:10.1016/j.jacc.2008.07.067

PRE-CLINICAL RESEARCH

Molecular Imaging of Interstitial Alterations in Remodeling Myocardium After Myocardial Infarction

Susanne W. M. van den Borne, MD,*† Satoshi Isobe, MD, PHD,* Johan W. Verjans, MD,* Artiom Petrov, PHD,* Dagfinn Lovhaug, MSC,‡ Peng Li, MD, PHD,* H. Reinier Zandbergen, MD,* Youping Ni, MD, PHD,* Peter Frederik, PHD,† Jun Zhou, MD,* Bente Arbo, PHD,‡ Astri Rogstad, PHD,‡ Alan Cuthbertson, PHD,‡ Salah Chettibi, PHD,‡ Chris Reutelingsperger, PHD,† W. Matthijs Blankesteijn, PHD,† Jos F. M. Smits, PHD,† Mat J. A. P. Daemen, MD, PHD,† Faiez Zannad, MD, PHD, FACC,§ Mani A. Vannan, MD, FACC,* Navneet Narula, MD,* Bertram Pitt, MD, FACC,‖ Leonard Hofstra, MD, PHD,† Jagat Narula, MD, PHD, FACC*

Irvine, California; Maastricht, the Netherlands; Oslo, Norway; Nancy, France; and Ann Arbor, Michigan

Objectives The purpose of this study was to evaluate interstitial alterations in myocardial remodeling using a radiolabeled Cy5.5-RGD imaging peptide (CRIP) that targets myofibroblasts.

Background Collagen deposition and interstitial fibrosis contribute to cardiac remodeling and heart failure after myocardial infarction (MI). Evaluation of myofibroblastic proliferation should provide indirect evidence of the extent of fibrosis.

Methods Of 46 Swiss-Webster mice, MI was induced in 41 by coronary artery occlusion, and 5 were unmanipulated. Of the 41 mice, 6, 6, and 5 received intravenous technitium-99m labeled CRIP for micro–single-photon emission computed tomography imaging 2, 4, and 12 weeks after MI, respectively; 8 received captopril or captopril with losartan up to 4 weeks after MI. Scrambled CRIP was used 4 weeks after MI in 6 mice; the remaining 10 of 46 mice received unradiolabeled CRIP for histologic characterization.

Results Maximum CRIP uptake was observed in the infarct area; quantitative uptake (percent injected dose/g) was highest at 2 weeks (2.75 ± 0.46%), followed by 4 (2.26 ± 0.09%) and 12 (1.74 ± 0.24%) weeks compared with that in unmanipulated mice (0.59 ± 0.19%). Uptake was higher at 12 weeks in the remote areas. CRIP uptake was histologically traced to myofibroblasts. Captopril alone (1.78 ± 0.31%) and with losartan (1.13 ± 0.28%) significantly reduced tracer uptake; scrambled CRIP uptake in infarct area (0.74 ± 0.17%) was similar to CRIP uptake in normal myocardium.

Conclusions Radiolabeled CRIP allows for noninvasive visualization of interstitial alterations during cardiac remodeling, and is responsive to antiangiotensin treatment. If proven clinically feasible, such a strategy would help identify post-MI patients likely to develop heart failure. (J Am Coll Cardiol 2008;52:2017–28) © 2008 by the American College of Cardiology Foundation

Heart failure (HF) is evolving as 1 of the most important cardiovascular health problems worldwide. In the U.S. alone, approximately 5 million people suffer from manifest HF and more than 500,000 new cases are diagnosed every year (1). The syndrome of HF post-myocardial infarction (MI) is characterized by a relentless course of myocardial remodeling and functional deterioration (2–4), which continues to occur even after the initial causative injury has abated (5,6). In addition to the replacement fibrosis in the region of MI, interstitial fibrosis in the noninfarcted myocardium significantly contributes to the adverse remodeling and HF (7). In fact, presence of fibrosis remote from the infarct zone accounts for two-thirds of the fibrous tissue in the cardiomyopathic heart (7–10). The magnitude of myo-

See page 2029

From the *University of California, Irvine School of Medicine, Irvine, California; †Cardiovascular Research Institute Maastricht, Maastricht University, Maastricht, the Netherlands; ‡GE Healthcare, AS, Oslo, Norway; §University Henri Poincaré, Nancy, France; and the ‖University of Michigan, Ann Arbor, Michigan. Dagfinn Lovhaug and Drs. Arbo, Rogstad, Cuthbertson, and Chettibi, who prepared the tracer for the imaging studies, are employees of GE Healthcare. Dr. Pitt is a consultant to Pfizer, Merck, Takeda, AstraZeneca, Synvista, Novartis, and Nile Therapeutics, but has no conflicts directly with the project. Dr. van den Borne was supported by a grant from the Van Walree Fund of the Royal Netherlands Academy of Arts and Sciences. Dr. Verjans was partially supported by the DiPalma-Brodsky research grant to Dr. Jagat Narula. CRIP and scrambled CRIP were kindly provided to Dr. Jagat Narula by GE Healthcare, Oslo, Norway. Drs. van den Borne and Isobe contributed equally to this study. Joel S. Karliner, MD, served as Guest Editor for this article.

Manuscript received April 30, 2008; revised manuscript received July 31, 2008, accepted July 31, 2008.

Abbreviations and Acronyms

ASMA = alpha smooth muscle actin
CRIP = Cy5.5-RGD imaging peptide
CT = computed tomography
HF = heart failure
LV = left ventricle/ventricular
MI = myocardial infarction
PBS = phosphate-buffered saline
RGD = arginine-glycine-aspartate
SPECT = single-photon emission computed tomography
Tc = technetium

cardial fibrosis is correlated to the extent of ventricular dysfunction (11). It is conceivable that an ability to noninvasively detect the process of myocardial fibrosis would allow assessment of the likelihood of evolution of HF after MI.

Collagen production and fibrosis in the myocardium are associated with myofibroblastic proliferation (5). Myofibroblasts demonstrate up-regulation of angiotensin receptors and integrin moieties, which, in turn, may promote collagen genes and reduce metalloproteinase genes (12). Such effects of integrin up-regulation are prevented by abrogation of autocrine transforming growth factor-β signaling (12). The RGD peptide (containing the arginine-glycine-aspartate motif) that binds to integrins such as $\alpha_v\beta_3$ has been used to identify neovascularization in post-infarct animal models (13). Since integrin $\alpha_v\beta_3$ is associated with the supermature focal adhesions on the cell membrane of myofibroblasts, we hypothesized that appropriately labeled RGD probes should identify myofibroblasts in post-infarct myocardium (14). In addition, scrutiny of the pro-collagen I sequence revealed RGD binding domains, such as DDX, and could also constitute a target for RGD-based imaging. Therefore, uptake of RGD probe should indirectly represent the rate of fibrogenesis or collagen deposition.

In the present study, we used Cy5.5-RGD imaging peptide (CRIP) labeled with technetium (Tc)-99m, for feasibility of imaging the process of active myocardial fibrosis in a murine model of post-MI ventricular dysfunction. The noninvasive imaging ability of the radiolabeled probe was compared with echocardiographic parameters of left ventricular (LV) geometric changes and pathologic characterization of interstitial alterations. The fluorescent moiety of the targeting peptide allowed better histologic characterization of the probe localization. An antibody against the fluorescent moiety of CRIP was used to immunoelectron microscopically trace the localization of CRIP. In addition, in vitro experiments were performed for characterization of the CRIP binding to mature and pro-collagen.

Methods

Experimental myocardial infarction in mice. The experimental protocol was approved by the Institution Animal Care and Use Committee of the University of California, Irvine, School of Medicine. In 41 adult Swiss Webster male mice (age: 4 months; body weight: ~50 g), MI was induced under pentobarbital (75 mg/kg) and isoflurane gas anesthesia (2.0% to 3.0%) using a stereomicroscope (Leica MZ FL III, Leica, Switzerland). For this purpose, animals were placed on a heating pad in the supine position, endotracheal intubation was performed under direct laryngoscopy, and mechanical ventilation was maintained with a small animal respirator (Harvard Apparatus, Holliston, Massachusetts) (tidal volume = 1.0 ml, rate = 120 breaths/min). After thoracotomy, the lateral branch of the left coronary artery was ligated with a 6.0-silk suture 3 to 4 mm below the tip of the left atrium. Successful ligation was verified by visual inspection of the LV apex for myocardial blanching, indicating interruption in coronary flow. The chest cavity was closed in layers with 6.0-silk, and the skin closed with 4.0-silk sutures. Animals were gradually weaned from the respirator.

For evaluation of serial changes in collagen synthesis by radiolabeled CRIP imaging, animals were divided into groups at 2 weeks (n = 6), 4 weeks (n = 6), and 12 weeks (n = 5) after infarction (Table 1). Two groups of 4 animals each were treated with either captopril (60 mg/kg/day) alone or in combination with losartan (captopril 30 mg/kg/day, losartan 10 mg/kg/day) dissolved in the drinking water, to evaluate if molecular imaging with CRIP would allow determination of efficacy of therapeutic intervention. Five unmanipulated control mice were subjected to CRIP imaging for comparison with the infarcted mice after a 4-week wait. In addition, 6 animals, 4 weeks after MI, were imaged with Tc-labeled scrambled peptide (scrambled CRIP) to ensure the specificity of CRIP. In the remaining 10 mice, nonradiolabeled CRIP was used for pathologic characterization of the target using fluorescence microscopy and immunoelectron microscopy.

Echocardiography. All animals were subjected to extensive echocardiographic studies for the assessment of myocardial infarct size, LV cavity dimensions, and ventricular function.

Echocardiographic examination was performed under 2% isoflurane anesthesia for the assessment of infarct size, LV cavitary dimensions, and ventricular function before nuclear imaging. Echocardiograms were recorded with a commercially available ultrasound system (Sequoia, Siemens,

Table 1 Classification of Animals Used in the Study

						4 Weeks, n	
Probe	Label	Control, n	2 Weeks, n	4 Weeks, n	12 Weeks, n	Captopril	Captopril + Losartan
Cy5.5-RGD	Tc	5	6	6	5	4	4
Cy5.5-RGD	—	—	10	—	—	—	—
Cy5.5 scrambled	Tc	—	—	6	—	—	—

RGD = arginine-glycine-aspartate; Tc = technetium.

Mountain View, California) using a 14-MHz linear probe (15L8, Siemens). An advanced high frame rate imaging technique, acoustic capture (Paragon, Siemens), was adopted for image acquisition allowing temporal resolution of 8 to 10 ms (frame rate, 100 to 120/s). B-mode images of LV parasternal long- and short-axis views at base, mid, and apical LV levels were digitally stored as movie loops in 2 to 3 cardiac cycle lengths. Still images of LV M-mode as well as pulsed-wave Doppler spectrum of mitral valve inflow and aortic valve forward flow were acquired at a sweep of 100 mm/s. Infarct and LV area were measured by tracing endocardial borders on long-axis images, and infarct-to-LV ratio was calculated. LV wall thicknesses and cavity dimensions were measured on LV M-mode spectrum as recommended by the American Society of Echocardiography guidelines (15), followed by calculation of percent fractional shortening and ejection fraction.

CRIP and scrambled CRIP: structure and radiolabeling. CRIP and scrambled CRIP were the kind gift of GE Healthcare, AS, Oslo, Norway. CRIP (AH110863) (Fig.1) is a 2.5-kD peptide conjugated to both a fluorescent cyanine dye Cy5.5 and the chelating agent cPN216; the latter is linked for radiolabeling of the peptide with ^{99m}Tc. The peptide comprises 10 amino acids, contains an RGD-motif, and has a bicyclic structure formed by a disulfide and a thioether bridge. The dye moiety and the chelating agent are conjugated to the peptide via the side-chain of lysine residue at the N- and C-terminal ends, respectively. A scrambled version of CRIP (AH112298) was also prepared, in which the order of the amino acids in CRIP was altered so that the sequence did not express an RGD-motif. The dye and the chelating agent were conjugated at the same positions.

For radiolabeling, 50 μg of tracer was dissolved in 50 μl of MeOH and then added to a freeze-dried kit. One milliliter of $^{99m}TcO_4^-$ was added to the compound and left at room temperature for 20 to 30 min. Radiolabeling was confirmed by instant thin-layer chromatography with radiopurity of more than 90%. For nuclear imaging, 170 ± 18 MBq (4.6 ± 0.4 mCi) of Tc-CRIP was injected through the tail vein and imaging was performed after 3.5 h.

Micro–single-photon emission computed tomography (SPECT) imaging with Tc-CRIP and micro-computed tomography (CT). Radionuclide imaging was performed using a dual-head micro-SPECT gamma camera with micro-CT (X-SPECT, Gamma Medica, Inc., Northridge, California) under isoflurane anesthesia. In vivo micro-SPECT images of the heart were acquired in a 64 × 64 scaffold, 32 steps at 120 s/step on a 140-keV photopeak of ^{99m}Tc with a 15% window using a low-energy, high-resolution, pinhole collimator. After SPECT acquisition, micro-CT images were acquired without moving the mice. The micro-CT used an X-ray tube operating at 50 kVp and 0.6 mA, and images were acquired for 0.5 s/view for 256 views in 360° rotation. The micro-SPECT images were

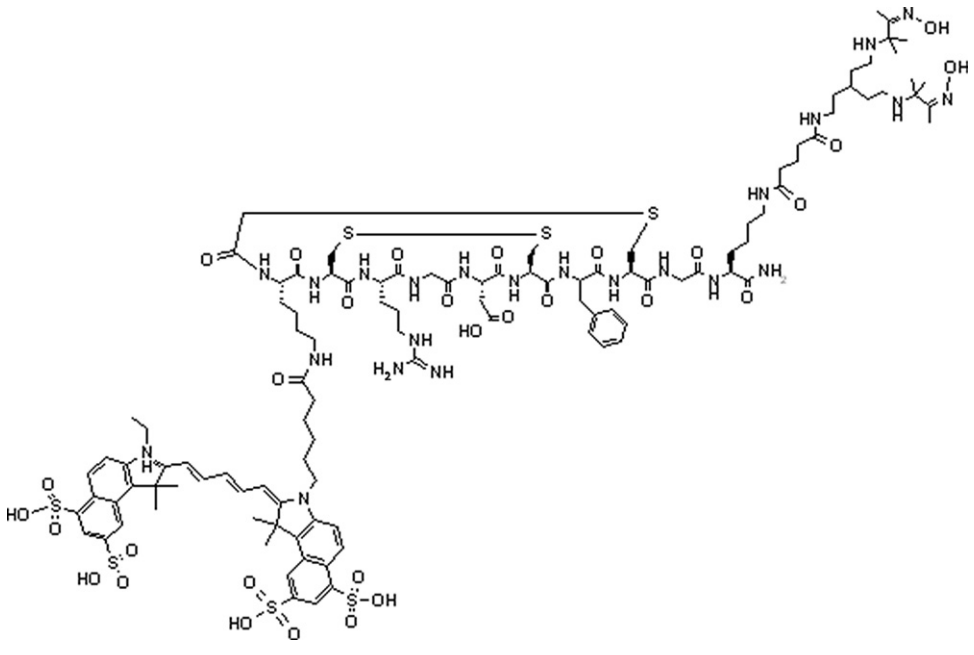

Figure 1 The Structure of CRIP

CRIP is a 2.5-kD, 10-amino acid peptide, which contains an arginine-glycine-aspartate (RGD)-motif and has a bicyclic structure formed by a disulfide bridge and a thioether bridge. It is conjugated to both a fluorescent cyanine dye (Cy5.5) and the chelating agent cPN216 for radiolabeling with technetium-99m; the dye moiety and the chelating agent are conjugated through the lysine side-chain at the N- and C-terminal ends, respectively. For preparation of scrambled CRIP, the order of the amino acids in CRIP was mixed so the sequence did not express the RGD-motif; the dye and the chelating agent were conjugated similarly (not shown).

converted to 256 × 256 scaffold and micro-CT studies were fused, allowing simultaneous scintigraphic and anatomic information in all tomographic scans in 3 different axes. After in vivo imaging, animals were sacrificed with an overdose of pentobarbital (150 mg/kg). Hearts were carefully explanted, and planar images of ex vivo heart were acquired for 15 min in a 128 × 128 matrix using a low-energy, high-resolution, pinhole collimator. Thereafter, hearts were cut into 3 bread-loaf slices (infarct, peri-infarct, and remote regions), using a mouse heart matrix (Zivic Laboratories, Inc., Pittsburgh, Pennsylvania). The quantitative radiotracer uptake was determined by a gamma scintillation counter (1480 Wizard 3, Wallac Co., Waltham, Massachusetts). Biodistribution studies for the lung, liver, spleen, and kidney uptake were also undertaken.

Histopathologic characterization of myocardial specimens. After the nuclear imaging studies, the apical (predominantly containing infarct tissue), mid myocardium (peri-infarct), and basal (predominantly containing noninfarcted remote tissue) myocardial slices were washed in phosphate-buffered saline (PBS), fixed overnight with 4% paraformaldehyde in PBS (pH 7.4 at 4°C), and stored in PBS with 0.02% sodium azide at 4°C until used. The specimens were further processed by dehydration in a graded series of ethanol for paraffin-embedding. The blocks were cut in 5-μm sections, transferred to Vectabond (Vector Laboratories, Burlingame, California) reagent-treated slides (Vector SP-1800, Vector Laboratories), dried overnight, and stored until ready for use.

Masson's trichrome staining was used to determine infarct size. After deparaffinization and rehydration, sections were placed in working Weigert's iron hematoxylin for 10 min and tepid water rinsed for 10 min. Tissue sections were then incubated in Biebrich scarlet-acid fuchsin solution for 5 min, differenced in phosphotungstic-phosphomolybdic acid for 5 min, and stained in aniline blue for 8 min. After rinsing with 1% gallic acetic acid, sections were dehydrated and mounted in permanent mount medium.

Sirius red staining eliminates cytoplasmic staining, revealing thin septa and collagen fibers clearly, and enabling quantitative morphometric measurements. Sections were treated in 0.2% aqueous phosphomolybdic acid for 5 min and subsequently incubated for 60 min with 0.1% sirius red F3BA (C.I. 35780, Polysciences, Northhampton, United Kingdom) in saturated picric acid and washed for 2 min with 0.01 N HCl. Sections were rinsed in 70% alcohol for 30 s, then dehydrated and mounted with a cover-slip, and the amount of collagen was quantified (16). The quality of collagen fibers was further investigated by sirius red polarization microscopy, allowing semiquantification of the mature, thick, tightly packed orange/red fibers and the newly formed, thin, loosely assembled fibers as yellow/green (17–20).

Alpha smooth muscle actin (ASMA) was used to determine myofibroblasts in the infarct area. After deparaffinization, rehydration, and blocking of endogenous peroxidase, sections were incubated for 2 h at room temperature using anti-ASMA (ASMA monoclonal antibody, Sigma, St. Louis, Missouri, dilution 1:2,000). After washing in PBS, sections were incubated with secondary antibody (rabbit antimouse horseradish peroxidase, 1:500, DAKO, Carpinteria, California) for 1 h at room temperature. Sections were briefly counterstained with hematoxylin.

Fluorescence microscopy. For localization of the target sites for CRIP, nonradiolabeled probe was injected intravenously in animals with 2-week-old MI. After 3.5 h, mice were sacrificed and hearts were excised. Frozen sections of 5 μm were cut and rehydrated in PBS. Sections were incubated for 2 h at room temperature using anti-ASMA antibody (1:2,000, Sigma). After washing in PBS, sections were incubated with secondary antibody for 1 h at room temperature (donkey antimouse IgG FITC, Jackson ImmunoResearch Europe, Newmarket, Suffolk, United Kingdom). Sections were examined using a Nikon Eclipse E-800 microscope (Nikon Instruments Europe B. V., Amstelveen, the Netherlands).

In vitro studies for CRIP binding. Modified enzyme-linked immunoadsorbent assays were developed for defining the interaction of CRIP and collagen I and III (Sigma Aldrich, St. Louis, Missouri). In addition, a pro-collagen I peptide was custom constructed containing a DDX sequence (H2N-GPP-GKN-G*DD*-*G*EA-GKP-GR-COOH). This sequence is common for mouse and human pro-collagen I. The analysis was conducted using a Biacore 3000 system (Biacore, GE Healthcare, Uppsala, Sweden) that enabled detection of noncovalent interactions between CRIP and pro-collagen I peptide in real time, applying the physical principle of surface plasmon resonance. The analysis involved immobilization of synthetic peptide sequence on sensor chips CM5, followed by assessment of soluble CRIP or scrambled CRIP to the immobilized ligand. The change in refractive index at the chip surface layer, as the soluble components associated with the ligand and subsequently dissociated, was expressed as resonance units. To compensate for nonspecific background binding, an unmodified control surface was used. The change in resonance units at this surface was subtracted from the change in resonance units at the ligand surface.

Immunoelectron microscopy. Immunoelectron microscopy was performed according to previously described methods (21). In short, hearts were perfused with 0.2% glutaraldehyde in 2% paraformaldehyde and 0.1 mol/l phosphate buffer, pH 7.4. Hearts were excised and stored for 60 min in the previously mentioned solution before storage in 1% paraformaldehyde and 0.1 mol/l phosphate buffer, pH 7.4 at 4°C for at least 24 h. Tissue samples were stored in 2.3 mol/l sucrose in 0.1 mol/l phosphate buffer, and sections were cut and placed on a grid in methyl cellulose/2.3 mol/l sucrose solution (1:1). Anticyanine antibody was used (Acris Antibodies, Hiddenhausen, Germany) to ultrastructurally trace CRIP localization. After protein A gold labeling, sections were examined using a Philips CM100 microscope (Eindhoven, the Netherlands).

Statistical analysis. To determine the statistical significance of differences in quantitative scintigraphic data, echocardiographic parameters, and histopathologic observations, 1-way analysis of variance was performed followed by post-hoc Bonferroni test for multiple comparisons. Correlations were determined using linear regression analysis. Due to the small number of mice in each group, the assumptions of the 1-way analysis of variance and linear regression models should be regarded as exploratory rather than definitive. The p values of <0.05 were considered statistically significant.

Results

CRIP: target affinity and localization characteristics. Probe localization characteristics were determined by fluorescence microscopy of myocardial tissue sections of hearts explanted 2 weeks after MI from animals injected with (nonradiolabeled) CRIP (Fig. 2). Uptake was observed predominantly in the myocardial infarct zone. Colocalization of ASMA in the same cells as CRIP-positive cells by fluorescence microscopy suggested the probe specificity for myofibroblasts. Similarly, immunoelectron microscopic examination was performed wherein intravenously administered CRIP in 2-week-old infarcts was localized by immunogold-labeled anticyanine antibody. Uptake was confirmed in the myofibroblasts, which were ultrastructurally identified by the presence of large amounts of rough endoplasmic reticulum. A small amount of internalized CRIP was seen within the myofibroblasts. No uptake of the probe was observed in the externalized collagen fibers. In vitro binding assays revealed CRIP uptake by activated $\alpha_v\beta_{3/5}$ with an affinity of 1-3nM, but not by typical collagen receptors such as $\alpha_1\beta_1$ or $\alpha_5\beta_1$ or platelet receptor $\alpha_{II}\beta_3$. Also, CRIP did not bind to mature collagen type I or III fibers. However, a specific noncovalent interaction of CRIP was observed with a custom-made DDX-sequence containing pro-collagen I peptide (Fig. 2).

Radionuclide imaging with Tc-CRIP. The infarct size in all untreated animals was similar (Table 2). The LV cavity dimensions (both end-systolic and diastolic) were greater at 2, 4, and 12 weeks post-MI, and the percent fractional shortening and ejection fraction decreased post-MI compared with those in normal control animals. In vivo micro-SPECT imaging demonstrated Tc-CRIP uptake in the infarct area (Fig. 3). The use of micro-CT identified precise localization of the radioactivity in the cardiac region and allowed differentiation of the uptake in apical myocardium from radiotracer sequestration in the liver. Ex vivo planar images of the explanted heart specimens confirmed the results of in vivo imaging and demonstrated maximum uptake in infarct and border zones. Minimal increase in uptake was seen in the remote area (Fig. 4). In contrast to CRIP, scrambled CRIP did not show uptake in the infarcted myocardium, showing that CRIP uptake is RGD-dependent and -specific. Similarly, no Tc-CRIP uptake was seen in the unmanipulated hearts.

Uptake in the infarcted region was maximal in the 2-week-old MI. There was statistically significant reduction in uptake in 4- and 12-week-old infarcts (Fig. 4). Quantitative Tc-CRIP uptake in the myocardial tissue specimens was calculated and represented as percent injected dose/g (%ID/g) of tissue. It can be presumed that the quantitative uptake represents the extent of the process of myocardial fibrosis. As observed in the in vivo and ex vivo images, the maximum radiotracer uptake was observed in the infarcted myocardium (%ID/g: $2.75 \pm 0.46\%$) at 2 weeks, which was 5-fold higher than the control myocardial specimens ($0.59 \pm 0.19\%$; $p < 0.0001$) (Fig. 4B). This uptake was significantly higher compared with specimens from 4 ($2.26 \pm 0.17\%$; $p < 0.0038$) and 12 ($1.74 \pm 0.24\%$; $p < 0.0001$) weeks after MI. The CRIP uptake in the remote myocardium was higher than that in the control myocardial specimens, and it increased significantly by 12 weeks ($1.04 \pm 0.13\%$), as compared with uptake in control myocardial specimens ($0.68 \pm 0.16\%$; $p = 0.001$). The uptake in the infarct area had no correlation with MI size determined either by akinetic echo segments or Masson trichrome staining ($r = -0.17, -0.12$ respectively; $p =$ NS). The nontarget organ distribution of Tc-CRIP demonstrated the kidney to be the major organ of radiation burden (and excretion) (Online Appendix). The tracer clearance was fast, and only 8% of the tracer could be recovered in circulation at 2 h as compared with 5 min after administration; CRIP T1/2 was calculated as 28 min.

Two additional groups of 4 animals each were treated with either captopril alone or in combination with losartan. Upon ultrasound examination, the neurohumoral antagonists prevented ventricular dilation and preserved ventricular function (Table 2). The CRIP uptake at 4 weeks after MI was significantly reduced after captopril ($1.78 \pm 0.31\%$; $p = 0.0004$) or captopril + losartan ($1.13 \pm 0.28\%$; $p = 0.0001$) treatment compared with uptake in untreated animals (Fig. 5).

Histopathologic assessment. The histologic sections demonstrated large infarcts involving the anterior LV wall (Fig. 6); infarct size was similar in all animals. During the 3 months following infarction, the LV wall demonstrated significant thinning and the extent of inflammation gradually subsided. Myofibroblasts, expressing ASMA, were present at 2 weeks post-MI in the infarct area and decreased over time. Replacement and interstitial collagen was analyzed by picrosirius red polarization microscopy of myocardial specimens (Fig. 7) obtained from infarct and remote regions. Although the total collagen content in the infarct region remained similar over time, the thin, newly formed (yellow/green) collagen fibers reduced and correlated with the radiotracer uptake ($r^2 = 0.34$; $p = 0.05$) (Figs. 7A, 7C, and 7E). In the remote region, overall collagen deposition was markedly lower compared with that in the infarct region (Figs. 7A and 7B). However, both collagen content and (yellow/green) thin collagen fibers increased in the remote region over time (Fig. 7D). There was a direct correlation

JACC Vol. 52, No. 24, 2008
December 9, 2008:2017–28

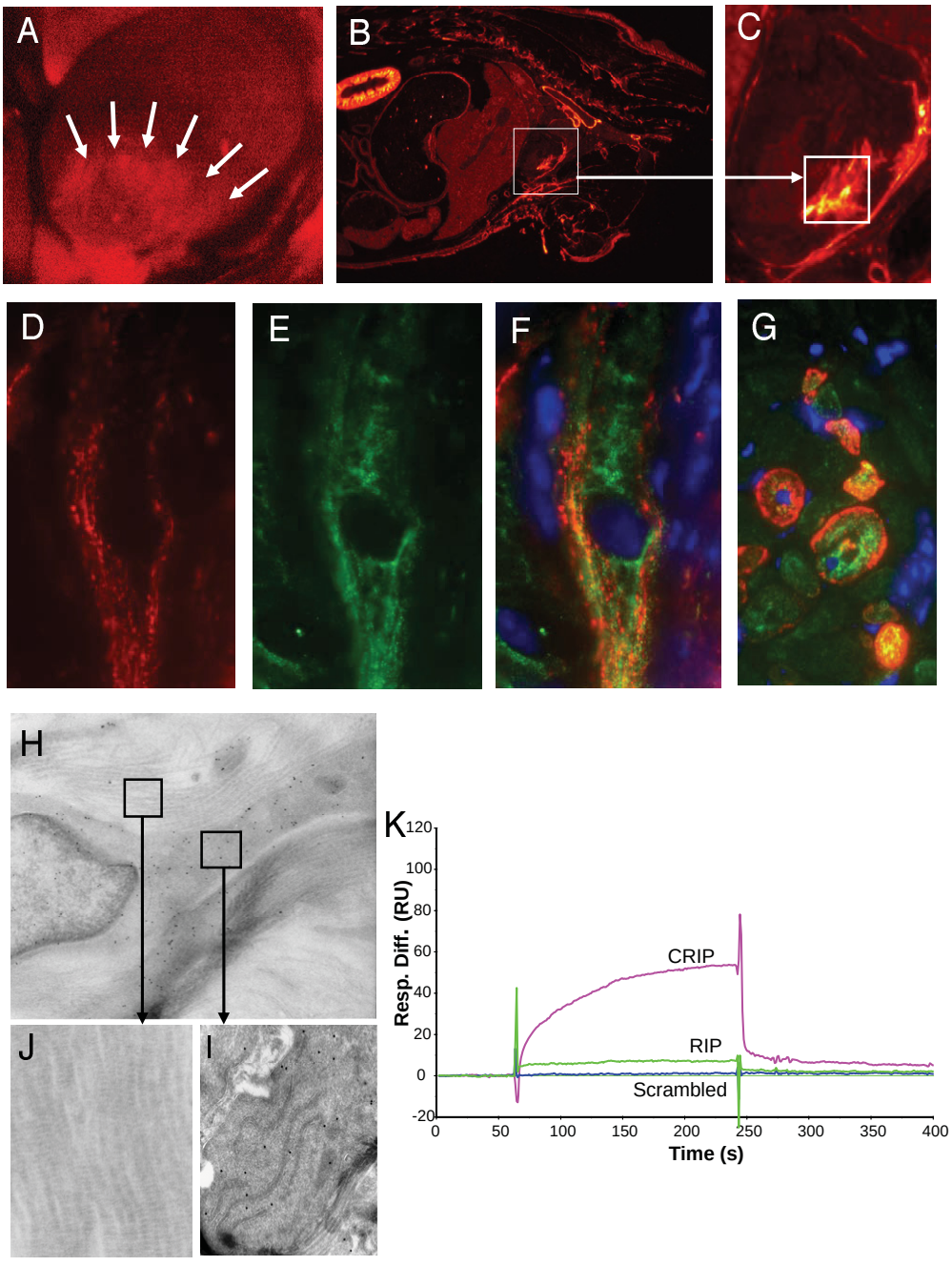

Figure 2 **Characterization of Target Binding of CRIP**

Probe targeting was evaluated 3.5 h after intravenous administration of Cy5.5-RGD imaging peptide (CRIP) in 2-week post-myocardial infarction (MI) animals. Localization of the Cy5.5 fluorescence **(red)** was clearly observed in the infarct and peri-infarct zones in vivo **(A, arrows)**. A 30-μ whole mouse slice demonstrates myocardial uptake of the probe **(B, square)**; intense uptake is seen in the kidney, which serves as the route of excretion. **(C)** Magnification of the area enclosed by the **box** in **panel B** demonstrates fluorescent probe localization in the subendocardium. **(D to G)** For further characterization of the probe targets, we correlated the uptake of intravenously administered CRIP in 2 week post-MI animals **(red, D)** with concurrent staining of the sections by anti-alpha smooth muscle actin (ASMA) antibody **(green, E)**, colocalization is shown by **overlay (F)**. The localization of CRIP was observed in spindle-shaped myofibroblasts in the infarct area. CRIP and ASMA colocalization is seen in transversely sectioned myofibroblasts in **(G)**. For immunoelectron microscopy, intravenously administered CRIP was traced by gold labeled anticyanine antibody (black immunogold particles, 10 nm). CRIP clearly localized with myofibroblasts **(H)**, containing a characteristic abundance of rough endoplasmic reticulum **(I)**. No uptake was seen in mature collagen fibers outside of myofibroblasts **(J)**; **(K)** sensograms (Biacore 3000 instrument) obtained with CRIP and scrambled CRIP exposure to a surface with an immobilized DDX peptide sequence H2N-GPP-GKN-GDD-GEA-GKP-GR-COOH, aa221-240 from pro-collagen I. In addition, arginine-glycine-aspartate (RGD) imaging peptide without Cy5.5 dye was used in the experiment (RIP). The higher resonance unit values for CRIP than RIP are due to the higher molecular weight of CRIP.

Table 2 Echocardiographic Parameters of LV Remodeling and Function

Parameter	Normal Control	2 Weeks	4 Weeks	12 Weeks	4 Weeks	
					Captopril	Captopril + Losartan*
n	5	6	6	5	4	4
HR (beats/min)	386 ± 55	476 ± 43†	406 ± 48‡	405 ± 63‡	324 ± 30	376 ± 106
MI (%)	0	47 ± 14†	48 ± 10†	47 ± 12†	38 ± 16	31 ± 13
LVDd (cm)	0.46 ± 0.03	0.53 ± 0.03†	0.49 ± 0.05	0.6 ± 0.06§	0.5 ± 0.07	0.5 ± 0.06
LVDs (cm)	0.29 ± 0.03	0.48 ± 0.03†	0.44 ± 0.06†	0.51 ± 0.08†	0.4 ± 0.1	0.39 ± 0.1
FS (%)	38 ± 4	11 ± 4†	11 ± 5†	14 ± 7†	29 ± 9§	24 ± 12
EF (%)	74 ± 5	27 ± 9†	29 ± 11†	34 ± 14†	41 ± 6	47 ± 15

Data are presented as mean ± SD. *Treatment groups were statistically compared with 4 weeks post-MI. †$p < 0.05$ versus normal control, ‡$p < 0.05$ versus 2 weeks, §$p < 0.05$ versus 4 weeks. EF = ejection fraction; FS = fractional shortening; HR = heart rate; LV = left ventricle; LVD = left ventricle diameter (s = systolic, d = diastolic); MI = myocardial infarction/left ventricle area × 100%.

between tracer uptake and the thin collagen fiber deposition ($r^2 = 0.45$; $p = 0.001$) (Fig. 7F). The direct correlation of CRIP uptake with ASMA-positive myofibroblasts and thin collagen fibers suggests that collagen production is decreased in the infarct zone over time.

Discussion

The present study demonstrates the feasibility of noninvasive assessment of interstitial alterations in post-infarction ventricular myocardium by Tc-99m labeled CRIP. The lack of binding of scrambled CRIP (which carries a deranged RGD-motif) confirmed that the CRIP binding is RGD-dependent and specific. Fluorescence and immunoelectron microscopy confirmed the binding of CRIP to the myofibroblasts. The CRIP uptake paralleled newly formed, thin, yellow/green collagen fiber production, suggesting that the CRIP uptake should indirectly represent the rate of collagen deposition. CRIP did not bind to the mature collagen fibers.

The uptake of CRIP in the infarct area was significantly higher at 2 weeks compared with that at 4 or 12 weeks after MI; the uptake almost completely resolved by 52 weeks in the infarct area (data not shown). The time-response curve of CRIP uptake in post-MI hearts may parallel the expression dynamics of $\alpha_v\beta_3$, as observed in hepatic stellate cells (22). Myofibroblasts evolve and are activated by inflammatory cytokines elicited in the area following the insult. Collagen and other matrix molecules are produced, and integrins are up-regulated to attach the cells to the matrix for survival and proliferation. The expression of β_3 integrins is associated with angiogenesis in the peri-infarct zone and peaks around 7 days after MI as part of the remodeling process. Subsequently, as inflammation resolves, collagen fibrils are cross linked by transglutaminase activity, no more ligands are available for $\alpha_v\beta_3$ binding, and the cells disappear through apoptosis or anoxis (22). Therefore, after 12

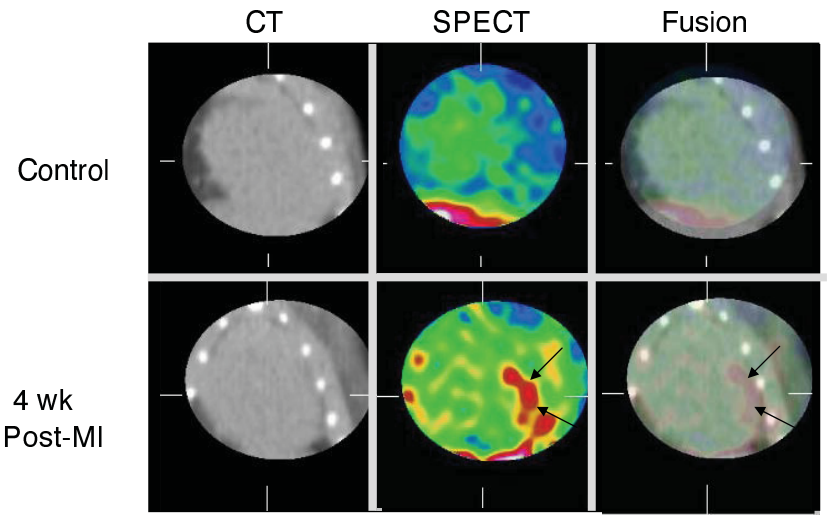

Figure 3 In Vivo Micro-CT, Micro-SPECT, and Fusion Images in Frontal Projection in Unmanipulated Control and 4-Week Post-MI Animals 3.5 h After Radiolabeled CRIP Administration

No uptake of technetium-labeled Cy5.5-RGD imaging peptide (Tc-CRIP) was observed in the unmanipulated animal **(top row)**. On the other hand, intense anterior uptake is seen in the infarcted mouse **(bottom row)**. The cardiac localization is confirmed in the computed tomography (CT) fusion image. MI = myocardial infarction; SPECT = single-photon emission computed tomography.

JACC Vol. 52, No. 24, 2008
December 9, 2008:2017–28

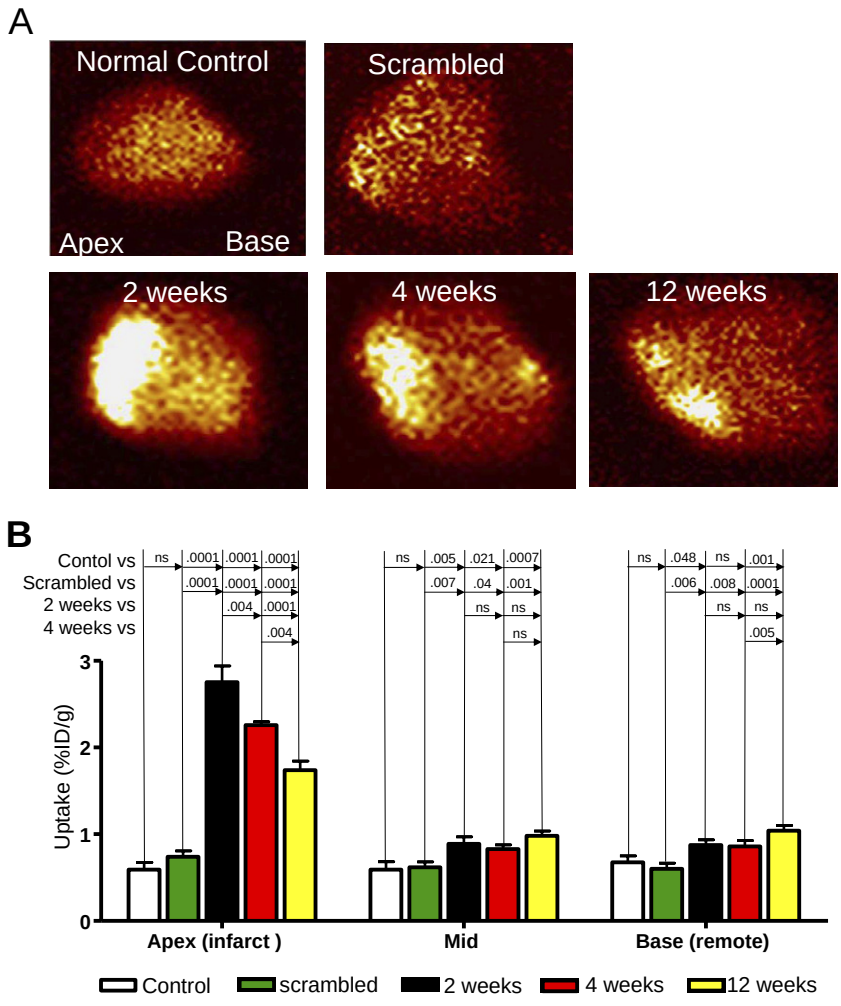

Figure 4 **Ex Vivo Images of the Explanted Hearts in Control and Post-MI Animals With Radiolabeled CRIP and Scrambled CRIP**

(A) Control heart with Cy5.5-RGD imaging peptide (CRIP) probe and 4-week post-myocardial infarction (MI) heart with scrambled CRIP show no radiotracer uptake. On the other hand, intense CRIP uptake is seen in 2-week post-MI animal. The uptake in the infarcted area was highest in mice 2 weeks after MI, followed by 4 and 12 weeks after MI. **(B)** Quantitative technetium-CRIP uptake in the infarct (apex), peri-infarct (mid), and remote (base) areas. The percent injected dose/g uptake in the infarct area is highest in mice 2 weeks after MI, followed by 4 and 12 weeks after MI. On the other hand, the uptake in peri-infarcted and remote areas shows trends toward higher uptake from 2 to 12 weeks after MI. No uptake of scrambled peptide was seen in the infarct zone. Quantitative data confirmed the findings of ex vivo images. Data are presented as mean ± standard error of the mean.

months there are large amounts of collagen, but no more integrins for CRIP to bind to; in other words, there is fibrosis, but little fibrogenesis or myofibroblasts in mouse infarcts. However, since myofibroblasts have been reported up to 20 years after MI in well-healed human infarcts (23), the binding characteristics of CRIP may be different in humans than in rodent hearts.

Unlike the infarcted zone, CRIP uptake in the remote myocardium was higher at 12 weeks. It is well established that alterations in interstitial collagen can significantly influence the size and shape of the cardiac chamber as well as ventricular function and hence, ventricular remodeling (24). Excessive collagen deposition or pathologic fibrosis contributes to LV dysfunction and poor prognosis in MI patients by inducing myocardial stiffness, promoting development of arrhythmias, and adversely affecting systolic function (25).

The myocardium contains an endogenous renin-angiotensin system, and activation of the renin-angiotensin-aldosterone axis results in cardiac fibroblast proliferation and fibrosis (26,27). This response is transduced by angiotensin receptors, which are far more abundant on cardiac fibroblasts than on myocytes (28). Angiotensin II acts through the up-regulation of additional fibrogenic growth factors, which mediate or augment the effects of angiotensin II, including transforming growth factor β_1. Up-regulation of angiotensin production, angiotensin II type 1 receptors, and increased collagen messenger ribonucleic acid in myofibro-

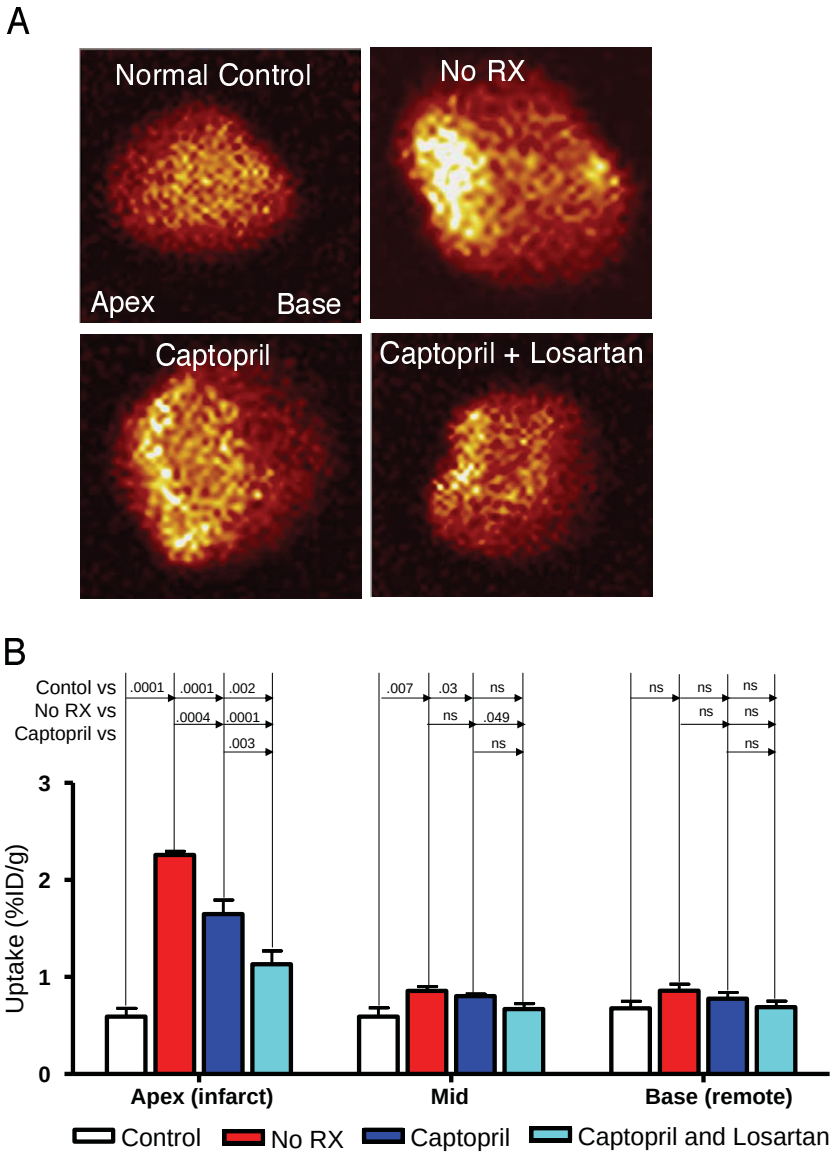

Figure 5 **Radiolabeled CRIP Uptake After Captopril and Losartan Treatment in Post-MI Animals**

In 4-week post-myocardial infarction (MI) animals, captopril treatment alone and in combination with losartan demonstrate significantly lower radiotracer uptake, as observed in gamma images of the explanted hearts **(A)**. Quantitative technetium-labeled Cy5.5-RGD imaging peptide (Tc-CRIP) uptake was significantly lower after therapeutic intervention in infarcted and nonsignificantly lower in noninfarcted areas **(B)**. Data are presented as mean ± standard error of the mean.

blasts is associated with healing infarct scars (29), and antiangiotensin therapy may prevent adverse myocardial remodeling. The uptake of Tc-CRIP was markedly reduced by captopril alone and more so in combination with losartan. Although angiotensin II levels decrease initially with angiotensin-converting enzyme inhibitor therapy (30,31), their levels may rise gradually over time due to alternative conversion pathways. Therefore, therapy with a combination of an angiotensin-converting enzyme inhibitor with an angiotensin receptor blocker acts synergistically and may have a benefit greater than that with either agent used alone. The present study demonstrates the relatively superior effect of combination therapy in reducing fibrogenesis compared with captopril therapy alone. Although the OPTIMAAL (Optimal Therapy in Myocardial Infarction with the Angiotensin II Antagonist Losartan) and the VALIANT (Valsartan in Acute Myocardial Infarction) studies did not substantiate the concept of combination therapy in post-MI patients (32,33), the Val-HeFT (Valsartan Heart Failure Trial) and CHARM (Candesartan in Heart Failure–Assessment of Reduction in Mortality and Morbidity) studies have demonstrated the superior efficacy of combination therapy in reduction of morbidity in HF patients with (CHARM Addition) (34) or without (Val-HeFT) (35) improvement in

JACC Vol. 52, No. 24, 2008
December 9, 2008:2017–28

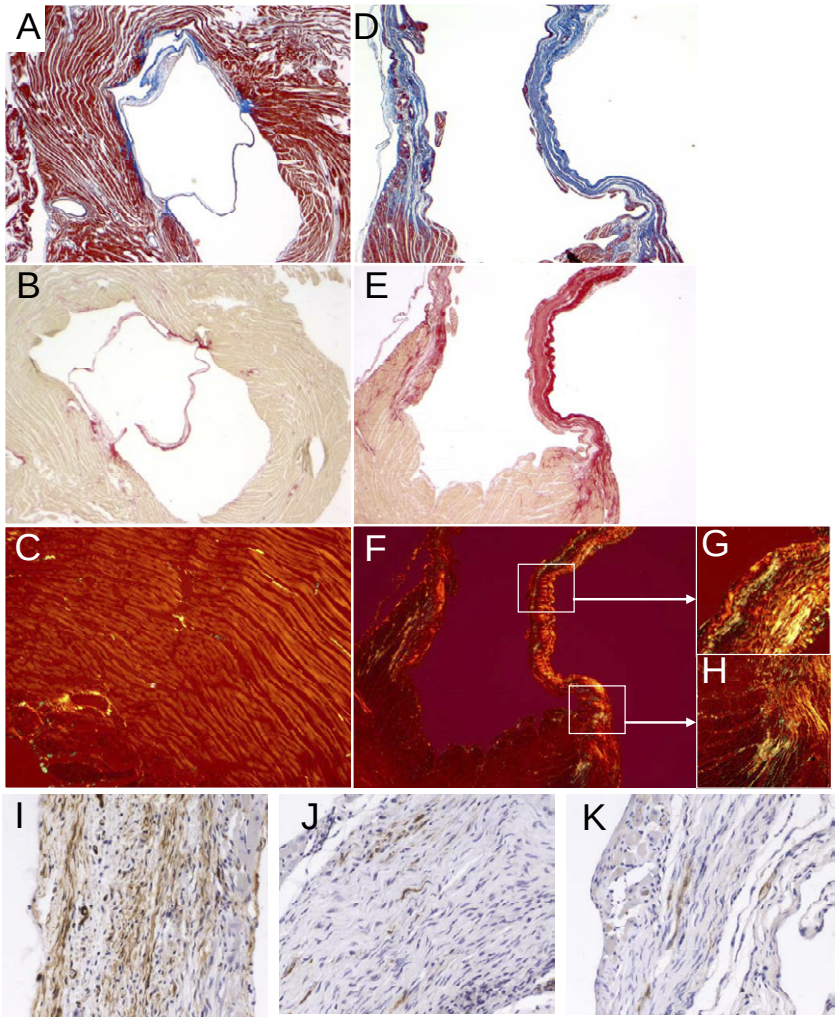

Figure 6 **Histopathological Characterization of Control and 4-Week Post-MI Hearts**

Masson's trichrome **(A, D)** and sirius red **(B, E)** staining, and sirius red staining with polarized light **(C, F to H)** in remote **(A to C)** and infarct center or border regions **(D to H)** in a heart 4 weeks after myocardial infarction (MI). The remote area is from the base of the heart as indicated by the enclosed mitral valve. The remote region shows minimal fibrosis **(A)** and collagen deposition **(B, C)**. On the other hand, the infarct region shows significant wall thinning and fibrosis **(D)**, with evidence of collagen deposition **(E, F)**. Two areas from **(F)** are magnified to demonstrate collagen deposition in the infarct center **(G)** and in the infarct border **(H)**. Immunohistochemical characterization with anti-alpha smooth muscle actin (ASMA) antibody **(brown)** of the infarct zone at 2 **(I)**, 4 **(J)**, and 12 **(K)** weeks reveals progressive decrease in the number of myofibroblasts over time.

survival. Since both agents are known to favorably alter prognosis in patients with HF and the present study demonstrates a decrease in collagen deposition after captopril with or without losartan treatment, it is possible that the decrease in collagen deposition is a favorable phenomenon. Alternatively, we hypothesize that the impact of antiangiotensin therapy on the infarct zone may be relatively lower as compared with that in the remote region, where all collagen formation may get abrogated. As such, evaluation of the impact of therapy at 12 weeks could have offered more information.

Since LV remodeling post-MI is the leading cause of HF and is a determinant of morbidity and mortality (3,36), it is important to predict the likelihood of occurrence of cardiac remodeling. It is possible to detect the occurrence of collagen formation post-MI by measuring pro-collagen I and III in serum. The measurements of these markers have been shown to provide independent information pertaining to LV function (37,38) and survival (39,40) in patients with HF. However, these markers are not specific and may not be of value in patients with other conditions associated with collagen formation, such as arthritis (41). The potential value of radiolabeled CRIP is its ability to noninvasively localize at the site of interstitial alterations and collagen formation in the myocardium, and therefore may provide information about the evolution of HF. Our pilot clinical study with a radiolabeled RGD peptide in patients at 3 and 8 weeks after MI has shown the feasibility of interstitial imaging. In these patients, a 1-year follow-up

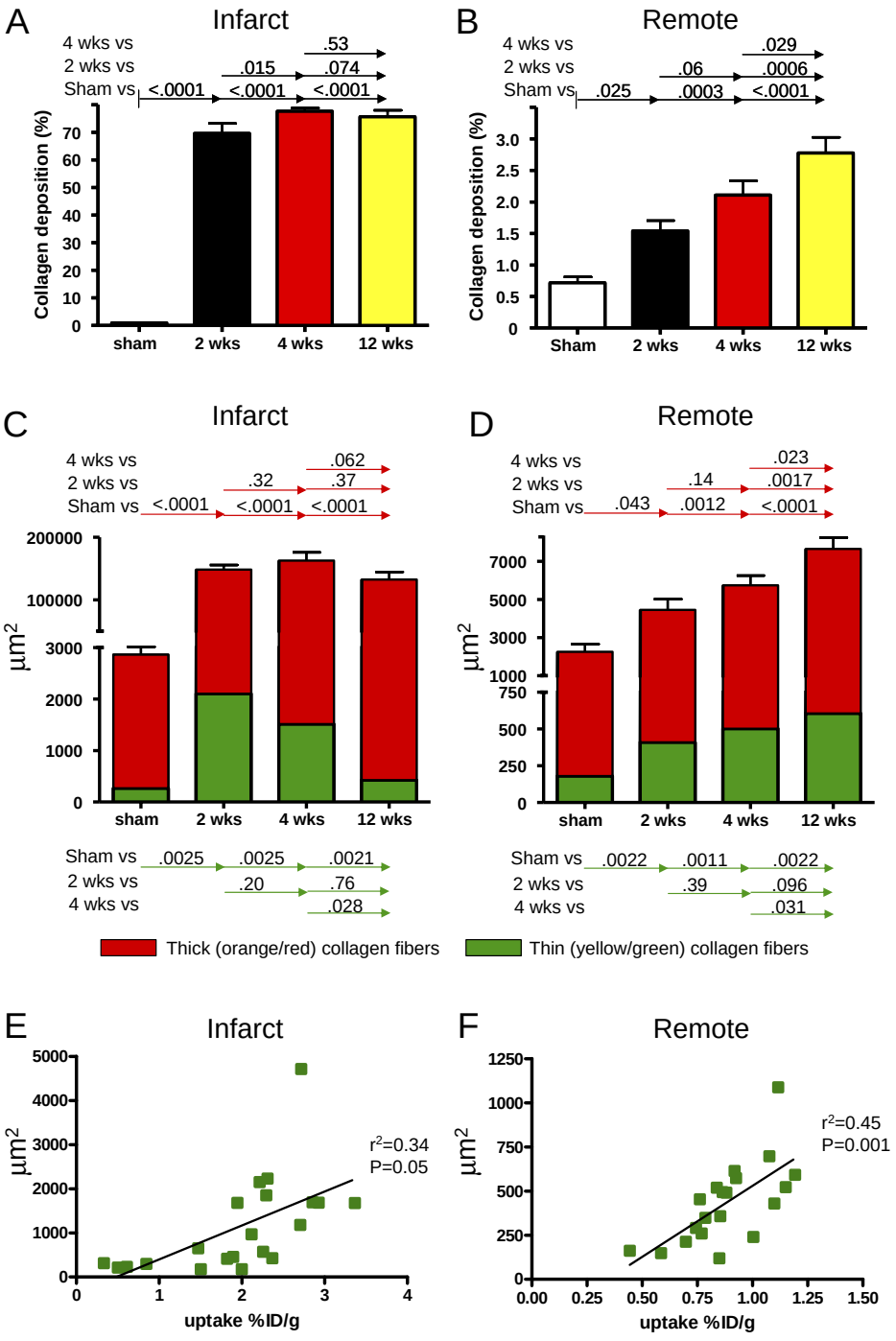

Figure 7 **Collagen Fiber Analysis in Infarct and Remote Regions**

The total collagen content in the infarcted area **(A)** remains similar with the passage of time; it increases significantly in the remote region **(B)**. Characterization of the collagen fibers by polarization reveals that the thin or new collagen fibers **(green)** decreased in the infarct region (suggestive of cessation of collagen production and maturation of the collagen fibers) **(C)** and increased substantially in the remote area **(D)** (suggesting ongoing production of the new collagen with increasing total collagen content). The prevalence of new collagen fibers paralleled the Cy5.5-RGD imaging peptide (CRIP) uptake and demonstrated a significant direct correlation, both in infarct and remote zones **(E, F)**.

magnetic resonance imaging study confirmed the extent of fibrosis detected earlier by the radiolabeled RGD uptake (42).

Acknowledgment

The authors thank Hans Duimel for his help with the immunoelectron microscopy.

JACC Vol. 52, No. 24, 2008
December 9, 2008:2017–28

Reprint requests and correspondence: Dr. Jagat Narula, Division of Cardiology, University of California, Irvine School of Medicine, 101 The City Drive, Building 53, Mail Route 81, Orange, California 92868-4080. E-mail: narula@uci.edu

REFERENCES

1. Thom T, Haase N, Rosamond W, et al. Heart disease and stroke statistics–2006 update: a report from the American Heart Association Statistics Committee and Stroke Statistics Subcommittee. Circulation 2006;113:e85–151.
2. Opie LH, Commerford PJ, Gersh BJ, Pfeffer MA. Controversies in ventricular remodelling. Lancet 2006;367:356–67.
3. Pfeffer MA, Braunwald E. Ventricular remodeling after myocardial infarction. Experimental observations and clinical implications. Circulation 1990;81:1161–72.
4. Pfeffer JM, Pfeffer MA, Braunwald E. Influence of chronic captopril therapy on the infarcted left ventricle of the rat. Circ Res 1985;57:84–95.
5. Cleutjens JP, Blankesteijn WM, Daemen MJ, Smits JF. The infarcted myocardium: simply dead tissue, or a lively target for therapeutic interventions. Cardiovasc Res 1999;44:232–41.
6. Volders PG, Willems IE, Cleutjens JP, Arends JW, Havenith MG, Daemen MJ. Interstitial collagen is increased in the non-infarcted human myocardium after myocardial infarction. J Mol Cell Cardiol 1993;25:1317–23.
7. Beltrami CA, Finato N, Rocco M, et al. Structural basis of end-stage failure in ischemic cardiomyopathy in humans. Circulation 1994;89:151–63.
8. Massie BM, Conway M. Survival of patients with congestive heart failure: past, present, and future prospects. Circulation 1987;75:IV11–9.
9. Gerdes AM, Capasso JM. Structural remodeling and mechanical dysfunction of cardiac myocytes in heart failure. J Mol Cell Cardiol 1995;27:849–56.
10. Francis GS, McDonald KM. Left ventricular hypertrophy: an initial response to myocardial injury. Am J Cardiol 1992;69:3G–7G, discussion 7G–9G.
11. Heeneman S, Cleutjens JP, Faber BC, et al. The dynamic extracellular matrix: intervention strategies during heart failure and atherosclerosis. J Pathol 2003;200:516–25.
12. Asano Y, Ihn H, Yamane K, Jinnin M, Mimura Y, Tamaki K. Increased expression of integrin alpha(v)beta3 contributes to the establishment of autocrine TGF-beta signaling in scleroderma fibroblasts. J Immunol 2005;175:7708–18.
13. Meoli DF, Sadeghi MM, Krassilnikova S, et al. Noninvasive imaging of myocardial angiogenesis following experimental myocardial infarction. J Clin Invest 2004;113:1684–91.
14. Hinz B. Masters and servants of the force: the role of matrix adhesions in myofibroblast force perception and transmission. Eur J Cell Biol 2006;85:175–81.
15. Schiller NB, Shah PM, Crawford M, et al. Recommendations for quantitation of the left ventricle by two-dimensional echocardiography. American Society of Echocardiography Committee on Standards, Subcommittee on Quantitation of Two-Dimensional Echocardiograms. J Am Soc Echocardiogr 1989;2:358–67.
16. Heymans S, Luttun A, Nuyens D, et al. Inhibition of plasminogen activators or matrix metalloproteinases prevents cardiac rupture but impairs therapeutic angiogenesis and causes cardiac failure. Nat Med 1999;5:1135–42.
17. Whittaker P, Kloner RA, Boughner DR, Pickering JG. Quantitative assessment of myocardial collagen with picrosirius red staining and circularly polarized light. Basic Res Cardiol 1994;89:397–410.
18. MacKenna DA, Omens JH, McCulloch AD, Covell JW. Contribution of collagen matrix to passive left ventricular mechanics in isolated rat hearts. Am J Physiol 1994;266:H1007–18.
19. Szendroi M, Vajta G, Kovacs L, Schaff Z, Lapis K. Polarization colours of collagen fibres: a sign of collagen production activity in fibrotic processes. Acta Morphol Hung 1984;32:47–55.
20. Andrade GB, Riet-Correa F, Montes GS, Battlehner CN, Saldiva PH. Dating of fibrotic lesions by the Picrosirius-polarization method. An application using the lesions of Lechiguana (bovine focal proliferative fibrogranulomatous panniculitis). Eur J Histochem 1997;41:203–9.
21. Liou W, Geuze HJ, Slot JW. Improving structural integrity of cryosections for immunogold labeling. Histochem Cell Biol 1996;106:41–58.
22. Zhou X, Jamil A, Nash A, et al. Impaired proteolysis of collagen I inhibits proliferation of hepatic stellate cells: implications for regulation of liver fibrosis. J Biol Chem 2006;281:39757–65.
23. Willems IE, Havenith MG, De Mey JG, Daemen MJ. The alpha-smooth muscle actin-positive cells in healing human myocardial scars. Am J Pathol 1994;145:868–75.
24. Jugdutt BI, Amy RW. Healing after myocardial infarction in the dog: changes in infarct hydroxyproline and topography. J Am Coll Cardiol 1986;7:91–102.
25. Whittaker P, Boughner DR, Kloner RA. Role of collagen in acute myocardial infarct expansion. Circulation 1991;84:2123–34.
26. Pfeffer JM, Fischer TA, Pfeffer MA. Angiotensin-converting enzyme inhibition and ventricular remodeling after myocardial infarction. Annu Rev Physiol 1995;57:805–26.
27. Weber KT. Extracellular matrix remodeling in heart failure: a role for de novo angiotensin II generation. Circulation 1997;96:4065–82.
28. Gray MO, Long CS, Kalinyak JE, Li HT, Karliner JS. Angiotensin II stimulates cardiac myocyte hypertrophy via paracrine release of TGF-beta 1 and endothelin-1 from fibroblasts. Cardiovasc Res 1998;40:352–63.
29. Sun Y, Weber KT. Infarct scar: a dynamic tissue. Cardiovasc Res 2000;46:250–6.
30. Schieffer B, Wirger A, Meybrunn M, et al. Comparative effects of chronic angiotensin-converting enzyme inhibition and angiotensin II type 1 receptor blockade on cardiac remodeling after myocardial infarction in the rat. Circulation 1994;89:2273–82.
31. Wollert KC, Drexler H. The kallikrein-kinin system in post-myocardial infarction cardiac remodeling. Am J Cardiol 1997;80:158A–161A.
32. Dickstein K, Kjekshus J. Effects of losartan and captopril on mortality and morbidity in high-risk patients after acute myocardial infarction: the OPTIMAAL randomised trial. Optimal Trial in Myocardial Infarction with Angiotensin II Antagonist Losartan. Lancet 2002;360:752–60.
33. Pfeffer MA, McMurray JJ, Velazquez EJ, et al. Valsartan, captopril, or both in myocardial infarction complicated by heart failure, left ventricular dysfunction, or both. N Engl J Med 2003;349:1893–906.
34. McMurray JJ, Ostergren J, Swedberg K, et al. Effects of candesartan in patients with chronic heart failure and reduced left-ventricular systolic function taking angiotensin-converting-enzyme inhibitors: the CHARM-Added trial. Lancet 2003;362:767–71.
35. Cohn JN, Tognoni G. A randomized trial of the angiotensin-receptor blocker valsartan in chronic heart failure. N Engl J Med 2001;345:1667–75.
36. White HD, Braunwald E. Applying the open artery theory: use of predictive survival markers. Eur Heart J 1998;19:1132–9.
37. Poulsen SH, Host NB, Jensen SE, Egstrup K. Relationship between serum amino-terminal propeptide of type III procollagen and changes of left ventricular function after acute myocardial infarction. Circulation 2000;101:1527–32.
38. Radovan J, Vaclav P, Petr W, et al. Changes of collagen metabolism predict the left ventricular remodeling after myocardial infarction. Mol Cell Biochem 2006;293:71–8.
39. Zannad F, Radauceanu A. Effect of MR blockade on collagen formation and cardiovascular disease with a specific emphasis on heart failure. Heart Fail Rev 2005;10:71–8.
40. Cicoira M, Rossi A, Bonapace S, et al. Independent and additional prognostic value of aminoterminal propeptide of type III procollagen circulating levels in patients with chronic heart failure. J Card Fail 2004;10:403–11.
41. Kotaniemi A, Risteli J, Aho K, Hakala M. Increased type I collagen degradation correlates with disease activity in reactive arthritis. Clin Exp Rheumatol 2003;21:95–8.
42. Verjans JW, Wolters SL, Lax M, et al. Imaging avb3/b5 integrin upregulation in patients after myocardial infarction. Circulation 2007;116:II3288.

Key Words: myofibroblasts ■ integrins ■ interstitial fibrosis ■ radionuclide imaging ■ heart failure ■ coronary artery disease.

APPENDIX

For a table on the tracer uptake in organs and blood, please see the online version of this article.